

Jordan Journal of Physics

ARTICLE

On the Optimization of the Microstructure and Mechanical Properties of Al-Co-Cr-Cu-Fe-Ni-Ti –Based High Entropy Alloys

A.M. Manzoni^a, S. Singh^{a,b}, H.M. Daoud^c, R. Völkl^c, U. Glatzel^c and N. Wanderka^a

^a *Helmholtz-Zentrum Berlin für Materialien und Energie GmbH, Hahn-Meitner-Platz 1, D-14109 Berlin, Germany.*

^b *Department of Physics and Nanotechnology, SRM University, Kattankulathur, Kancheepuram Dt 603 203, India.*

^c *Metals and Alloys, University Bayreuth, Ludwig-Thoma-Str. 36b, D - 95447 Bayreuth, Germany.*

Received on: 31/1/2015; Accepted on: 13/4/2015

Abstract: Widely investigated AlCoCrCuFeNi high entropy alloy has been chosen for optimization of the microstructural and mechanical properties. Different paths have been chosen for optimization; namely the decrease of segregating element Cu, the increase of oxidation protective elements Al and Cr and the approach towards a γ - γ' microstructure as in Ni-based superalloys. Microscopical observation has been made for each optimization step and compared with results obtained by Vickers microhardness measurements. Out of five derivate alloys: AlCoCrFeNi, Al₂₃Co₁₅Cr₂₃Cu₈Fe₁₅Ni₁₆, Al₈Co₁₇Cr₁₇Cu₈Fe₁₇Ni₃₃, Al₈Co₁₇Cr₁₄Cu₈Fe₁₇Ni₃₃Mo₁Ti₁W₁ and Al₁₀Co₂₅Cr₈Fe₁₅Ni₃₆Ti₆, the most promising one has been chosen for further investigation.

Keywords: High entropy alloys; Microstructure; Transmission electron microscopy.

Introduction

For centuries, the concept of alloy creation has been based on the idea of having one base element and optimizing it with additional elements or at the most use binary alloys. This concept has already been broken by the discovery of metallic glasses, which consist of several elements none of which can be considered more important than the others. However, this notion has been restricted to amorphous materials, until the introduction of high entropy alloys or compositionally complex alloys at the beginning of the 21st century [1-2]. Since then, this new class of materials, consisting of five or more principal elements with close atomic radii, has been subject to intensive investigation all over the world. The family of elements that has been most observed

is Al-Co-Cr-Cu-Fe-Ni-Ti in various compositions [3-6].

The most outstanding property of high entropy alloys is their potential of forming single solid solutions. However, this has only been obtained in a very limited number of high entropy alloys [7-10] and is furthermore not the best option for good mechanical properties. Over time, it has been found that a two phase microstructure can lead to achieve better results. Several compositions and morphologies have been tried until an "optimum" morphology consisting of a disordered fcc matrix and ordered fcc precipitates has been chosen for future investigation.

This work focuses on the microstructural evolution from the "classic" equiatomic AlCoCrCuFeNi [11-14] alloy over AlCoCrFeNi

[15-16], $\text{Al}_{23}\text{Co}_{15}\text{Cr}_{23}\text{Cu}_8\text{Fe}_{15}\text{Ni}_{16}$ [17], $\text{Al}_8\text{Co}_{17}\text{Cr}_{17}\text{Cu}_8\text{Fe}_{17}\text{Ni}_{33}$ [17-18] and $\text{Al}_8\text{Co}_{17}\text{Cr}_{14}\text{Cu}_8\text{Fe}_{17}\text{Ni}_{33}\text{Mo}_1\text{Ti}_1\text{W}_1$ [19] to the optimized $\text{Al}_{10}\text{Co}_{25}\text{Cr}_8\text{Fe}_{15}\text{Ni}_{36}\text{Ti}_6$ alloy. The as-cast alloys have been investigated by optical microscopy, transmission electron microscopy (TEM) and three dimensional atom probe (3D-AP).

Experimental

The equiatomic alloys AlCoCrCuFeNi and AlCoCuFeNi have been melted in a vacuum levitation induction furnace. The elements were of 99.999% purity. The $\text{Al}_{23}\text{Co}_{15}\text{Cr}_{23}\text{Cu}_8\text{Fe}_{15}\text{Ni}_{16}$, $\text{Al}_8\text{Co}_{17}\text{Cr}_{17}\text{Cu}_8\text{Fe}_{17}\text{Ni}_{33}$, $\text{Al}_8\text{Co}_{17}\text{Cr}_{14}\text{Cu}_8\text{Fe}_{17}\text{Ni}_{33}$, $\text{Mo}_1\text{Ti}_1\text{W}_1$ and $\text{Al}_{10}\text{Co}_{25}\text{Cr}_8\text{Fe}_{15}\text{Ni}_{36}\text{Ti}_6$ alloys were cast in a vacuum induction furnace out of elements of 99.99% purity. All alloys were remelted several times in order to ensure homogeneity. The ingots were then cooled inside the furnace. Their mass was about 20 g.

Specimens for investigation with optical microscopy and hardness measurements were ground with different grinding papers and polished in three steps (3 μm and 1 μm diamond suspension) with a final polishing step consisting of 50 nm sized silica grains in a colloidal OP-U suspension. Some alloys were etched with an etching solution consisting of HCl , HNO_3 and H_2MoO_4 .

Discs of 3 mm diameter and 140 μm thickness were punched in order to prepare specimens for transmission electron microscopy (TEM) investigations. They were mechanically ground down to a thickness of about 110 μm and then electrochemically polished with a polishing solution of 83 % ethanol, 10 % perchloric acid and 7 % glycerine at -20°C and a voltage of 30 V. TEM investigations were made in a Philips CM30 with an acceleration voltage of 300 kV, equipped with an energy dispersive X-ray (EDX) detector by EDAX which is used to analyze the chemical composition of the phases.

Three-dimensional atom probe (3D-AP) measurements have been performed on two alloys; $\text{Al}_8\text{Co}_{17}\text{Cr}_{17}\text{Cu}_8\text{Fe}_{17}\text{Ni}_{33}$ and $\text{Al}_8\text{Co}_{17}\text{Cr}_{14}\text{Cu}_8\text{Fe}_{17}\text{Ni}_{33}\text{Mo}_1\text{Ti}_1\text{W}_1$. Specimens for 3D-AP investigations were first cut into rods of $0.2 \times 0.2 \times 10 \text{ mm}^3$ and then thinned down to a tip diameter of about 50 nm by using a final polishing solution of 98% butoxyethanol and 2% perchloric acid and a final voltage of 3 V. For more detailed information, see Ref. [15, 17]. The three-dimensional atom probe used in this study is a TAP, CAMECA instrument. The 3D-AP analyses were performed at a temperature of about 70 K with a pulse voltage fraction of 20% to the standing DC voltage and with a pulse repetition rate of 1000 Hz. Investigations are performed in a vacuum lower than 10^{-7} Pa.

Vickers microhardness measurements were carried out in Reichert-Jung MHT-10 microhardness tester with a load of ~ 0.5 N.

Results and Discussion

FIG. 1 shows a pseudo-ternary phase diagram (Al-Ti)-(Ni-Co)-Fe. It is a schematic view that aims at visualizing the fact that commercially used alloys are situated at the corner positions; i.e., having one (or sometimes two) base element, in this case, Al- or Ti-based, Fe-based or Ni- or Co-based. As Al and Ti shift the alloys' properties in the same direction and Ni and Co are also known to have similar behaviors, they have been grouped together. These elements have been chosen at the corners of the phase diagram, because most commercially used alloys are Al- or Ti- (blue circles), Co- or Ni- (green circles) or Fe-based (red circles). Some have a Fe-Ni binary basis (brown circles), but rare are the commercial alloys with three or more elements and a composition close to the equiatomic. The corresponding regions lie inside the orange circle and this is where the high entropy alloys (orange discs) of the present study are situated.

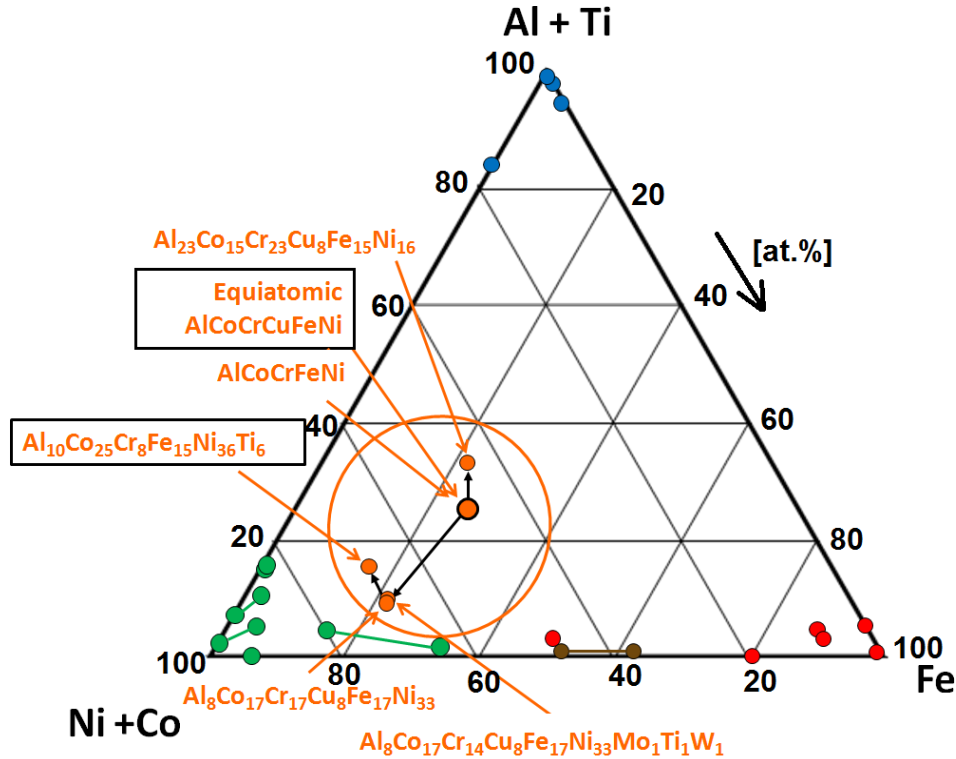


FIG. 1. A pseudo-ternary phase diagram (Al-Ti)-(Ni-Co)-Fe. Blue dots represent commercially used Al- or Ti-based alloys (e.g. the Al 4XXX series, the Al 8XXX series, Ti-B11007 or Ti-1Al-8V-5Fe), red dots commercially used Fe-based alloys (e.g. PH-13-8, X10 CrAlSi 24, the TRIP steels, 1RK91, X6 CrNi 22-13 or X10 NiCrAlTi 32-20), green dots commercially used Ni-based alloys (e.g. CMSX-4, CMSX-10, Waspaloy, Inconel 617, Stellite or Inconel 718) and brown dots Fe-Ni binary alloys (e.g. the Alloy 800). The investigated high entropy alloys are represented in orange. The black arrows point to the way of the alloy evolution.

The optimization path for AlCoCrCuFeNi has taken three ways, based on several well-known facts:

- Reduction of segregated phases. Cu-based phases segregate easily and can thus create disturbances inside the grains as well as at the grain boundaries → the Cu amount will be decreased ($\text{Al}_{23}\text{Co}_{15}\text{Cr}_{23}\text{Cu}_8\text{Fe}_{15}\text{Ni}_{16}$, $\text{Al}_8\text{Co}_{17}\text{Cr}_{17}\text{Cu}_8\text{Fe}_{17}\text{Ni}_{33}$, $\text{Al}_8\text{Co}_{17}\text{Cr}_{14}\text{Cu}_8\text{Fe}_{17}\text{Ni}_{33}\text{Mo}_1\text{Ti}_1\text{W}_1$) or removed completely (AlCoCrFeNi and $\text{Al}_{10}\text{Co}_{25}\text{Cr}_8\text{Fe}_{15}\text{Ni}_{36}\text{Ti}_6$).
- Optimize the oxidation properties of the alloy → the content of Al and Cr will be increased ($\text{Al}_{23}\text{Co}_{15}\text{Cr}_{23}\text{Cu}_8\text{Fe}_{15}\text{Ni}_{16}$).
- Preferential formation of a two-phase microstructure in the alloy. The microstructure of AlCoCrCuFeNi shows two main phases (except for the Cu-rich phases) with a tendency towards the well-known cubic microstructure in Ni-based alloys →

this features will be increased by increasing the amount of Ni and then fine-tuning by adjusting or adding other elements ($\text{Al}_8\text{Co}_{17}\text{Cr}_{17}\text{Cu}_8\text{Fe}_{17}\text{Ni}_{33}$, $\text{Al}_8\text{Co}_{17}\text{Cr}_{14}\text{Cu}_8\text{Fe}_{17}\text{Ni}_{33}\text{Mo}_1\text{Ti}_1\text{W}_1$ and $\text{Al}_{10}\text{Co}_{25}\text{Cr}_8\text{Fe}_{15}\text{Ni}_{36}\text{Ti}_6$).

FIG. 2 shows the optical micrographs of all six investigated alloys: AlCoCrCuFeNi, AlCoCrFeNi, $\text{Al}_{23}\text{Co}_{15}\text{Cr}_{23}\text{Cu}_8\text{Fe}_{15}\text{Ni}_{16}$, $\text{Al}_8\text{Co}_{17}\text{Cr}_{17}\text{Cu}_8\text{Fe}_{17}\text{Ni}_{33}$, $\text{Al}_8\text{Co}_{17}\text{Cr}_{14}\text{Cu}_8\text{Fe}_{17}\text{Ni}_{33}\text{Mo}_1\text{Ti}_1\text{W}_1$ and $\text{Al}_{10}\text{Co}_{25}\text{Cr}_8\text{Fe}_{15}\text{Ni}_{36}\text{Ti}_6$. All alloys show a dendritic morphology. In the case of $\text{Al}_{10}\text{Co}_{25}\text{Cr}_8\text{Fe}_{15}\text{Ni}_{36}\text{Ti}_6$ (FIG. 2f), the dendrites have the largest dimensions (up to 400 μm). In all cases (except for AlCoCrCuFeNi, FIG. 2a), a disturbingly large segregation of Cu could be avoided by the reduction of the Cu content or can be unmade by adequate heat treatments (e.g. 1250°C/1h in the case of $\text{Al}_8\text{Co}_{17}\text{Cr}_{17}\text{Cu}_8\text{Fe}_{17}\text{Ni}_{33}$ and $\text{Al}_8\text{Co}_{17}\text{Cr}_{14}\text{Cu}_8\text{Fe}_{17}\text{Ni}_{33}\text{Mo}_1\text{Ti}_1\text{W}_1$ [19]).

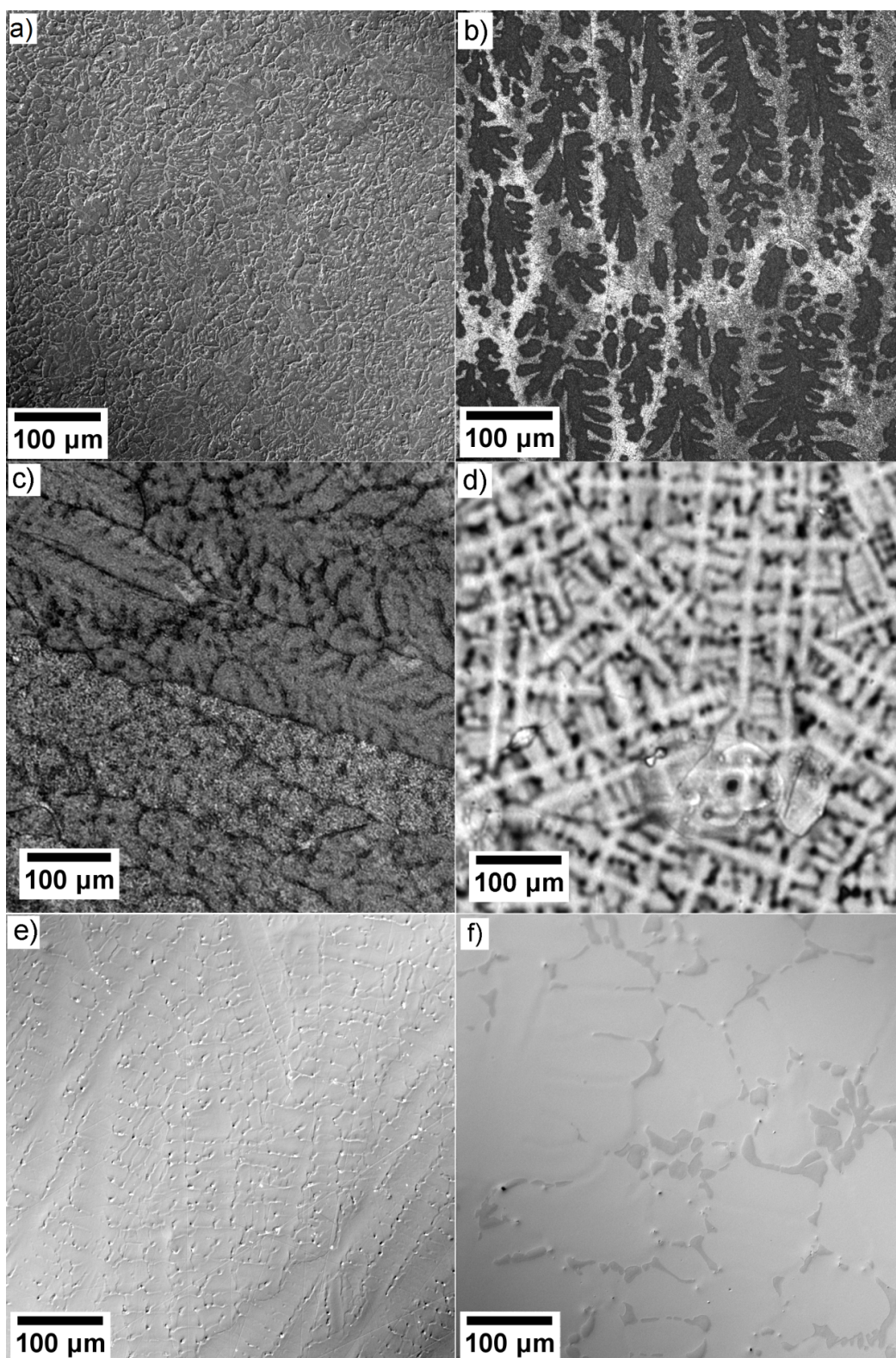


FIG. 2. Optical micrographs of a) AlCoCrCuFeNi (polished), b) AlCoCrFeNi (etched), c) $\text{Al}_{23}\text{Co}_{15}\text{Cr}_{23}\text{Cu}_8\text{Fe}_{15}\text{Ni}_{16}$ (etched), d) $\text{Al}_8\text{Co}_{17}\text{Cr}_{17}\text{Cu}_8\text{Fe}_{17}\text{Ni}_{33}$ (etched), e) $\text{Al}_8\text{Co}_{17}\text{Cr}_{14}\text{Cu}_8\text{Fe}_{17}\text{Ni}_{33}\text{Mo}_1\text{Ti}_1\text{W}_1$ (etched) and f) $\text{Al}_{10}\text{Co}_{25}\text{Cr}_8\text{Fe}_{15}\text{Ni}_{36}\text{Ti}_6$ (polished).

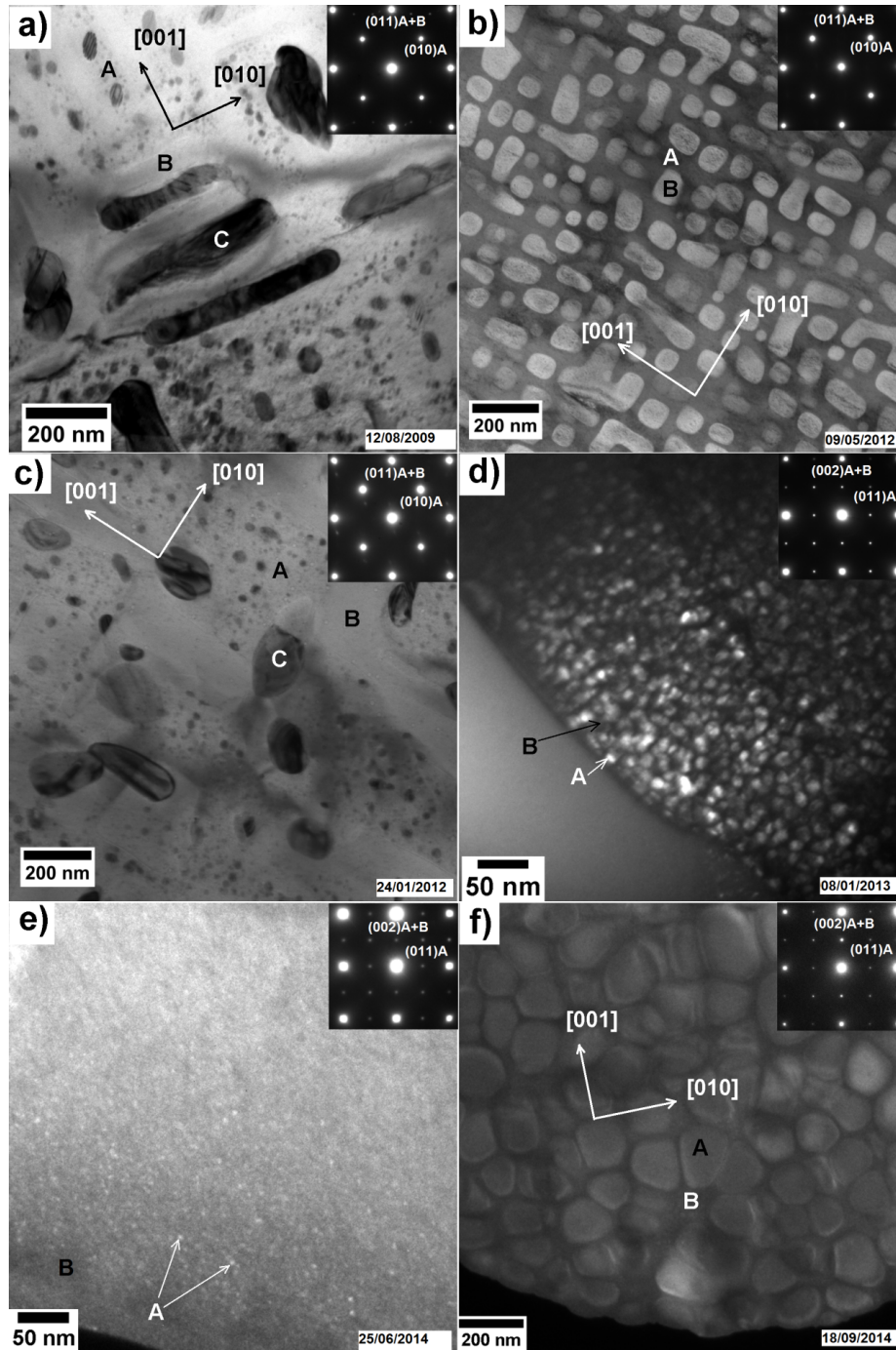


FIG. 3. TEM images of the dendritic regions of all investigated alloys: a) BF image of AlCoCrCuFeNi, at a random orientation, and a SAD taken along the [100] zone axis of the Al-Ni rich matrix and the Cr-Fe rich precipitate; b) BF of AlCoCrFeNi and the corresponding SAD taken along the [100] zone axis; c) BF of $\text{Al}_{23}\text{Co}_{15}\text{Cr}_{23}\text{Cu}_8\text{Fe}_{15}\text{Ni}_{16}$, at a random orientation, and a SAD taken along the [100] zone axis of the Al-Ni rich matrix and the Cr-Fe rich precipitate; d) DF of $\text{Al}_8\text{Co}_{17}\text{Cr}_{17}\text{Cu}_8\text{Fe}_{17}\text{Ni}_{33}$ and the corresponding SAD taken along the [100] zone axis; e) DF of $\text{Al}_8\text{Co}_{17}\text{Cr}_{14}\text{Cu}_8\text{Fe}_{17}\text{Ni}_{33}\text{Mo}_1\text{Ti}_1\text{W}_1$ and the corresponding SAD taken along the [100] zone axis; and f) DF of $\text{Al}_{10}\text{Co}_{25}\text{Cr}_8\text{Fe}_{15}\text{Ni}_{36}\text{Ti}_6$ and the corresponding SAD taken along the [100] zone axis. A stands for the Al-Ni rich phase, B for the Cr-Fe rich phase and C for the Cu-rich phase. In all SADs, two diffraction spots have been highlighted. One of them has a high intensity and belongs to both the ordered matrix and the disordered platelet. The other spot is a so-called superlattice spot which has a weaker intensity and thus belongs to only the Al-Ni rich matrix of ordered B2 structure. [010] and [001] directions have been indicated in the images in a), b), c) and f).

In order to gain information on a smaller scale, the alloys have been investigated by TEM. FIG. 3 shows bright or dark field images of the dendritic regions of the six alloys and selected area diffraction patterns (SADs) taken along the [100] zone axes of the matrix and the main precipitate. The bright field (BF) image of the original alloy AlCoCrCuFeNi (FIG. 3a) shows an Al-Ni rich matrix of B2 structure (called A), with 10 – 50 nm small Cu rich precipitates. Bright imaged Cr-Fe rich platelets of a disordered bcc phase (called B) as well as dark imaged Cu rich platelets of B2 structure (called C) can be distinguished [11]. This image has been taken along a direction which puts the Cu platelets in diffracting conditions. The SAD in the upper right corner has been taken along the [100] zone axis of the A-Ni rich matrix and the Cr-Fe rich platelets. The two highlighted diffraction spots belong to both the ordered matrix and the disordered platelet (in the case of the (011) spot) or only the Al-Ni rich matrix of ordered B2 structure (in the case of the (010) spot). The (010) superlattice spot can only be obtained from an ordered structure. FIG. 3b shows a BF image of AlCoCrFeNi, in which the bright imaged Cr-Fe rich precipitates of disordered bcc structure (B) can be distinguished inside a dark imaged matrix Al-Ni rich of B2 structure (A) [15]. The corresponding SAD has been taken in the same direction. FIG. 3c shows a BF image of Al₂₃Co₁₅Cr₂₃Cu₈Fe₁₅Ni₁₆. This microstructure is close to the one in AlCoCrCuFeNi: an Al-Ni rich matrix of B2 structure (A) with 10 – 200 nm Cu rich precipitates (C) and bright imaged Cr-Fe rich platelets of a disordered bcc structure (B) can be observed [17]. This image has been taken along a direction which puts the Cu platelets in diffracting conditions. The SAD in the upper right corner has been taken along the [100] zone axis of the A-Ni rich matrix and the Cr-Fe rich platelets. These three alloys are characterized by a global bcc structure.

FIG. 3d shows the DF image of Al₈Co₁₇Cr₁₇Cu₈Fe₁₇Ni₃₃. Note the different scale, at which a dark imaged matrix of almost nominal composition and disordered fcc structure (B) can be seen. The ~20 nm sized bright imaged precipitates are Al-Cu-Ni rich and present an L1₂ structure (A) [17]. The corresponding SAD has been taken in the same direction. In order to shift the melting point of the alloy to higher temperature and to increase the existing area of

the phase with the L1₂ structure, Mo, Ti and W were added to the alloy. However, Mo, Ti and W alter the microstructure of Al₈Co₁₇Cr₁₄Cu₈Fe₁₇Ni₃₃Mo₁Ti₁W₁ only slightly: FIG. 3e shows the DF image of Al₈Co₁₇Cr₁₄Cu₈Fe₁₇Ni₃₃Mo₁Ti₁W₁. The expected effect of the added elements was negligible. The precipitates are smaller than the ones observed in the Al₈Co₁₇Cr₁₇Cu₈Fe₁₇Ni₃₃ alloy: a dark imaged matrix of almost nominal composition and disordered fcc structure (B) with ~10 nm sized bright imaged Al-Cu-Ni rich precipitates with an L1₂ structure (A) [19]. The corresponding SAD has been taken in the same direction. The final alloy, Al₁₀Co₂₅Cr₈Fe₁₅Ni₃₆Ti₆, has a two-phase microstructure which is characterized by a matrix of a disordered fcc structure (B). The precipitates are Al-Ni-Ti rich and of L1₂ structure (A), but much bigger than in the two preceding alloys; namely up to 200 nm [20]. The corresponding SAD has been taken in the same direction. The last three alloys have a global fcc structure and show a γ - γ' morphology known from Ni-based alloys.

The microchemical compositions of the most important phases of the dendritic regions are summarized in Table 1. The main phases; namely the matrix and the most prominent precipitates, as well as the additional phases and some comments on the alloys' behaviors are summarized in Table 2.

In addition to the microstructural investigations, the alloys have been investigated for their microhardness. FIG. 4 shows the Vickers microhardnesses for the six alloys. The first three alloys of global bcc structure are much harder (> 400 HV) than the last three alloys of global fcc structure (< 350 HV). A high hardness is favorable, but unfortunately all three bcc alloys are too brittle for mechanical application. The complete removal of Cu as well as the addition of more Al and Cr do not seem to be a good path to follow for the optimization of AlCoCrCuFeNi.

The hardnesses of Al₈Co₁₇Cr₁₇Cu₈Fe₁₇Ni₃₃ and Al₈Co₁₇Cr₁₄Cu₈Fe₁₇Ni₃₃Mo₁Ti₁W₁ are too low, compared to Ni-based alloys (e.g. ~ 420 HV for CMSX4). However, the last alloy, Al₁₀Co₂₅Cr₈Fe₁₅Ni₃₆Ti₆ shows a medium hardness and the handling of the alloy during cutting and casting shows a promising ductility. This alloy will thus be kept for further optimization.

TABLE 1. Chemical composition of the main phases in the dendrites of the six investigated alloys AlCoCrCuFeNi, AlCoCrFeNi, Al₂₃Co₁₅Cr₂₃Cu₈Fe₁₅Ni₁₆, Al₈Co₁₇Cr₁₇Cu₈Fe₁₇Ni₃₃, Al₈Co₁₇Cr₁₄Cu₈Fe₁₇Ni₃₃Mo₁Ti₁W₁ and Al₁₀Co₂₅Cr₈Fe₁₅Ni₃₆Ti₆. Data have been taken from the references given in the Ref. column. The error bar is given by the standard deviation 2 σ .

Phase	Concentration [at.%]										Measuring method	Ref.
	Al	Co	Cr	Cu	Fe	Ni	W	Mo	Ti			
AlCoCrCuFeNi												
Al-Ni rich matrix	25.8 ± 3	17.9 ± 3	3.0 ± 3	10.4 ± 3	12.1 ± 3	30.8 ± 3						TEM/EDX [11]
Cr-Fe rich platelets	2.2 ± 3	20 ± 3	43.2 ± 3	0.3 ± 3	29 ± 3	5.3 ± 3						TEM/EDX [11]
Cu rich platelet	4.9 ± 3	1.8 ± 3	1.1 ± 3	85 ± 3	2.0 ± 3	5.2 ± 3						TEM/EDX [11]
AlCoCrFeNi												
Al-Ni rich matrix	32.0±3.4	22.6±2.0	4.9±1.4		13.0±1.1	27.5±2.6						TEM/EDX [15]
Cr-Fe rich precipitates	4.9±3.6	22.3±0.6	35.7±5.1		29.9±2.1	7.7±3.4						TEM/EDX [15]
Al₂₃Co₁₅Cr₂₃Cu₈Fe₁₅Ni₁₆												
Al-Ni rich matrix	28.9±1.5	21.2±1.1	10.3±3.1	6.1±0.4	12.6±1.1	20.8±1.3						TEM/EDX [17]
Cr-Fe rich platelets	3.8±0.3	13.3±1.1	50.1±3.0	2.3±0.9	26.0±0.9	4.6±1.6						TEM/EDX [17]
Cu rich phase	9.4±0.5	2.9±0.5	3.8±2.6	76.1±4.5	2.8±1.3	5.2±0.6						TEM/EDX [17]
Al₈Co₁₇Cr₁₇Cu₈Fe₁₇Ni₃₃												
Al-Ni rich precipitate	11.5±1.0	14.0±2.9	8.6±1.6	6.1±1.7	12.6±1.4	47.1±5.0						3D-AP [17]
Matrix	7.1±0.7	19.0±1.1	19.5±1.1	3.1±0.5	19.4±1.1	31.8±1.3						3D-AP [17]
Al₈Co₁₇Cr₁₄Cu₈Fe₁₇Ni₃₃Mo₁Ti₁W₁												
Al-Ni rich precipitate	20.4±0.6	13.4±0.7	7.8 ± 0.4	5.1 ± 0.2	11.3±1.1	39.4±1.2	0.1± 0.1	0.9±0.4	1.6 ± 0.2			3D-AP [19]
Matrix	8.0 ± 0.1	18.9±0.1	14.2±0.3	3.3 ± 0.1	18.3±0.2	35.8±0.4	0.2± 0.1	0.7 ± 0.1	0.7 ± 0.0			3D-AP [19]
Al₁₀Co₂₅Cr₈Fe₁₅Ni₃₆Ti₆												
Al-Ni rich matrix	12.1±1.4	22.3±0.9	3.1 ± 1.1	7.7 ± 1.7	45.5±2.9				9.3 ± 1.2			TEM/EDX This work
Cr-Fe rich platelets	8.8 ± 2.2	29.5±1.8	7.7 ± 1.2	20.0±4.2	30.7±4.3				3.2 ± 1.7			TEM/EDX This work

TABLE 2. Summary of the main phases and the additional phases as well as some comments on the six investigated alloys AlCoCrCuFeNi, AlCoCrFeNi, Al₂₃Co₁₅Cr₂₃Cu₈Fe₁₅Ni₁₆, Al₈Co₁₇Cr₁₇Cu₈Fe₁₇Ni₃₃, Al₈Co₁₇Cr₁₄Cu₈Fe₁₇Ni₃₃Mo₁Ti₁W₁ and Al₁₀Co₂₅Cr₈Fe₁₅Ni₃₆Ti₆.

As-cast alloy	Matrix (dendrite)	Main precipitating phase (dendrite)	Additional phases (dendrite)	Comments	Ref.
AlCoCrCuFeNi	Al-Ni rich, B2 structure	Cr-Fe rich, disordered bcc/	Cu rich phases of different shapes and structures	Too brittle for mechanical application	[11]
AlCoCrFeNi	Al-Ni rich, B2 structure	Cr-Fe rich, disordered bcc	-	Too brittle for mechanical application	[15]
Al ₂₃ Co ₁₅ Cr ₂₃ Cu ₈ Fe ₁₅ Ni ₁₆	Al-Ni rich, B2 structure	Cr-Fe rich, disordered bcc	Cu rich platelets	Too brittle for mechanical application	[17]
Al ₈ Co ₁₇ Cr ₁₇ Cu ₈ Fe ₁₇ Ni ₃₃	Cr-Co-Fe rich, disordered fcc	Al-Cu-Ni rich, L1 ₂ structure	-	Too soft for mechanical application	[17-18]
Al ₈ Co ₁₇ Cr ₁₄ Cu ₈ Fe ₁₇ Ni ₃₃ Mo ₁ Ti ₁ W ₁	Cr-Co-Fe rich, disordered fcc	Al-Cu-Ni rich, L1 ₂ structure	-	Too soft for mechanical application	[19]
Al ₁₀ Co ₂₅ Cr ₈ Fe ₁₅ Ni ₃₆ Ti ₆	Cr-Co-Fe rich, disordered fcc	Al-Ni-Ti rich, L1 ₂ structure	-	To be investigated	This work

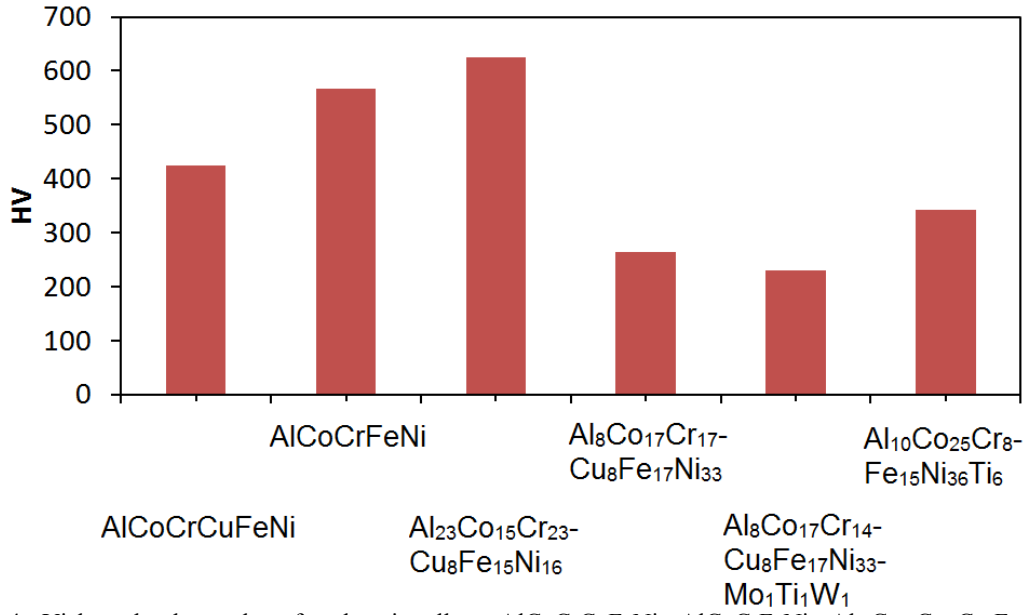


FIG. 4. Vickers hardness data for the six alloys AlCoCrCuFeNi, AlCoCrFeNi, Al₂₃Co₁₅Cr₂₃Cu₈Fe₁₅Ni₁₆, Al₈Co₁₇Cr₁₇Cu₈Fe₁₇Ni₃₃, Al₈Co₁₇Cr₁₄Cu₈Fe₁₇Ni₃₃Mo₁Ti₁W₁ and Al₁₀Co₂₅Cr₈Fe₁₅Ni₃₆Ti₆.

Summary

The initial high entropy alloy AlCoCrCuFeNi with equiatomic composition is characterized by a high number of phases and has insufficient mechanical properties, which inhibit the use of this alloy in the present state. Therefore, an optimization of this alloy has been achieved by the following steps:

- Reduction of segregated phases → the Cu content was reduced or removed completely.
- Optimization of the oxidation properties → the content of Al and Cr was increased.
- Preferential formation of a two-phase microstructure in the alloy → addition of Ti or variation of the composition of the other alloying elements. The microstructure shows the well-known γ - γ' microstructure.

The following high entropy alloys have been developed during the pathway of the optimization:

AlCoCrCuFeNi, AlCoCrFeNi, Al₂₃Co₁₅Cr₂₃Cu₈Fe₁₅Ni₁₆, Al₈Co₁₇Cr₁₇Cu₈Fe₁₇Ni₃₃, Al₈Co₁₇Cr₁₄Cu₈Fe₁₇Ni₃₃Mo₁Ti₁W₁ and Al₁₀Co₂₅Cr₈Fe₁₅Ni₃₆Ti₆. They have been investigated by optical, scanning electron microscopy and transmission electron microscopy as well as Vickers hardness measurements. The most promising alloy finally was found Al₁₀Co₂₅Cr₈Fe₁₅Ni₃₆Ti₆. However, further optimization of this alloy is necessary in order to increase its microhardness.

Acknowledgements

The authors are grateful to the German Research Foundation (DFG) for the financial support by WA 1378/15-2 and GL 181/25-2. The authors would like to thank C. Leistner for help with casting and C. Förster for sample preparation and help with hardness measurements.

References

- [1] Yeh, J.W., *Knowl. Bridge*, 40 (2003) 1.
- [2] Ranganathan, S., *Curr. Sci.*, 85 (2003) 1404.
- [3] Tong, C.J., Chen, M.R., Chen, S.K., Yeh, J.W., Shun, T.T., Lin, S.J. and Chang, S.Y., *Metall. Mater. Trans. A*, 36A (2005) 1263.
- [4] Jiang, L., Lu, Y.P., Dong, Y., Wang, T.M., Cao, Z.Q. and Li, T.J., *Intermetallics*, 44 (2014) 37.
- [5] Ng, C., Guo, S., Luan, J., Shi, S. and Liu, C.T., *Intermetallics*, 31 (2012) 165.
- [6] Chen, M.R., Lin, S.J., Yeh, J.W., Chen, S.K., Huang, Y.S. and Tu, C.P., *Materials Transactions*, 47 (2006) 1395.
- [7] Cantor, B., Chang, I.T.H., Knight, P. and Vincent, A.J.B., *Mater. Sci. Eng., A*, 375 (2004) 213.
- [8] Senkov, O.N., Wilks, G.B., Miracle, D.B., Chuang, C.P. and Liaw, P.K., *Intermetallics*, 18 (2010) 1758.
- [9] Shun, T.T., Hung, C.H. and Lee, C.F., *J. Alloys Compd.*, 493 (2010) 105.
- [10] Zhang, Y., Zhou, Y.J., Lin, J.P., Chen, G.L. and Liaw, P.K., *Adv. Eng. Mater.*, 10 (2008) 534.
- [11] Singh, S., Wanderka, N., Murty, B.S., Glatzel, U. and Banhart, J., *Acta. Mater.*, 59 (2011) 182.
- [12] Chen, H.Y., Tsai, C.W., Tung, C.C., Yeh, J.W., Shun, T.T., Yang, C.C. and Chen, S.K., *Annales De Chimie-Science Des Materiaux*, 31 (2006) 685.
- [13] Zhang, K.B., Fu, Z.Y., Zhang, J.Y., Shi, J., Wang, W.M., Wang, H., Wang, Y.C. and Zhang, Q.J., *J. Alloys Compd.*, 502 (2010) 295.
- [14] Tung, C.C., Yeh, J.W., Shun, T.T., Chen, S.K., Huang, Y.S. and Chen, H.C., *Mater. Lett.*, 61 (2007) 1.
- [15] Manzoni, A., Daoud, H., Völkl, R., Glatzel, U. and Wanderka, N., *Ultramicroscopy*, 132 (2013) 212.
- [16] Zhang, Y., Ma, S.G. and Qiao, J.W., *Metallurgical and Materials Transactions a-Physical Metallurgy and Materials Science*, 43A (2012) 2625.
- [17] Manzoni, A., Daoud, H., Mondal, S., van Smaalen, S., Völkl, R., Glatzel, U. and Wanderka, N., *J. Alloys Compd.*, 552 (2013) 430.
- [18] Daoud, H.M., Manzoni, A., Völkl, R., Wanderka, N. and Glatzel, U., *JOM*, 65 (2013) 1805.
- [19] Manzoni, A., Daoud, H., Völkl, R., Glatzel, U. and Wanderka, N., Submitted to *Ultramicroscopy*, (2015).
- [20] Daoud, H.M., Manzoni, A.M., Wanderka, N. and Glatzel, U., Submitted to *JOM*, (2015).